


## Inverse Grating Problem: Efficient Design of Anomalous Flexural Wave Reflectors and Refractors

Pawel Packo,<sup>1</sup> Andrew N. Norris,<sup>2</sup> and Daniel Torrent<sup>3,\*</sup>

<sup>1</sup>*Department of Robotics and Mechatronics, AGH University of Science and Technology, Aleja A. Mickiewicza 30, 30-059 Kraków, Poland*

<sup>2</sup>*Mechanical and Aerospace Engineering, Rutgers University, Piscataway, New Jersey 08854-8058, USA*

<sup>3</sup>*GROC, UJI, Institut de Noves Tecnologies de la Imatge, Universitat Jaume I, 12071 Castelló, Spain*

 (Received 5 September 2018; revised manuscript received 7 December 2018; published 11 January 2019)

We present an extensive formulation of the inverse grating problem for flexural waves in which the energy of each diffracted mode is selected and the grating configuration is then obtained by our solving a linear system of equations. The grating is designed as a lineal periodic repetition of a unit cell comprising a cluster of resonators attached at points whose physical properties are directly derived by inversion of a given matrix. Although both active and passive attachments can be required in the most-general case, it is possible to find configurations with only passive (i.e., damped) solutions. This inverse design approach is an alternative to the design of metasurfaces for flexural waves, overcoming the limitations of gradient phase metasurfaces, which require a continuous variation of the surface's impedance. When the grating is designed in such a way that all the energy is channeled into a single diffracted mode, it behaves as an anomalous refractor or reflector. The negative refractor is analyzed in depth, and it is shown that with only three scatterers per unit cell is it possible to build such a device with unitary efficiency.

DOI: [10.1103/PhysRevApplied.11.014023](https://doi.org/10.1103/PhysRevApplied.11.014023)

### I. INTRODUCTION

The fundamental property of gratings to redirect wave energy into multiple diffracted modes, transmitted and reflected, follows from simple considerations of interference effects. This can be seen with use of ray theory for the incident and diffracted directions combined with the unit spacing on the grating: diffraction modes correspond to multiples of  $2\pi$  in the phase difference of the incident and diffracted modes. However, the related multiple-scattering problem of calculating the distribution of diffracted wave energy among the modes is far more difficult, and the inverse problem of selecting a desired energy distribution among these orders has been scarcely considered so far. Recently, some approaches based on complex acoustic and electromagnetic scatterers [1–6] have been proposed for the design of gratings in which the energy is channeled toward a given direction. This provides an interesting alternative method to overcome the limitations of gradient metasurfaces [7], in which a continuous variation of the phase at the interface is required to accomplish the directional channeling. However, despite the recent interest in metagratings, a systematic method for the design of gratings with specific energy distribution between modes has so far not been presented.

Recently, Torrent [8] considered a general acoustic reflective grating and derived a linear relation between the grating parameters and the amplitudes of the diffracted orders. By selection of the diffracted amplitudes it is easy to obtain the grating parameters and therefore to solve the inverse problem. In this specific case drilled holes in an acoustically rigid surface were selected as the basic grating elements. The purpose of this work is to demonstrate that a similar inverse design approach may be applied to flexural waves in thin plates. Here the grating comprises a one-dimensional periodic repetition of a cluster of point attachments and the objective is to choose the number of these per unit cell and their mechanical parameters (effective impedance) so as to control the diffracted-wave amplitudes.

The scattering of flexural waves by point attachments and compact inhomogeneities and its applications have been widely studied in the literature. Plane-wave scattering from an array of finite points, an infinite line of equally spaced points, and from two parallel arrays is considered in Ref. [9]. Extensions to doubly infinite square and hexagonal arrays can be found in Refs. [10,11]. The hexagonal array introduces the possibility of Dirac cones in the dispersion surface, with implications for one-way edge waves [11,12]. A method for dealing with wave scattering from a stack of gratings, comprising parallel gratings with pinned circles in the unit cell, is given in Ref. [13] and used to

\*[dtorrent@uji.es](mailto:dtorrent@uji.es)

examine trapped modes in stacks of two gratings [13] and three gratings [14]. The scattering solution for a single grating is expressed in terms of reflection and transmission matrices, and recurrence relations are obtained for these matrices in the presence of a stack. Semi-infinite grating have recently been studied [15]. The addition of point scatterers to plates can produce flexural metamaterials with double-negative density and stiffness effective properties [16,17]. Scattering from a two-dimensional array of perforations in a thin plate designed to give high directivity for the transmitted wave is considered in Ref. [18]. Scattering of a Gaussian beam from a finite array of pinned points is examined in Ref. [19]. Time-domain solutions of flexural wave scattering from platonic clusters is considered in Ref. [20]. Infinite arrays of wave scatterers involve lattice sums for flexural waves, which, as we will see, is relevant to the present work. Lattice sums have other implications, for instance, in the context of an infinite square array of holes where the sums represent the consistency conditions between the local expansions at an arbitrary perforation and for the hole in the central unit cell [21], also known as ‘‘Rayleigh identities.’’

In this work we consider an infinite array of point scatterers with the unit cell comprising a cluster of  $N$  point scatterers characterized by scalar impedances. A schematic of the grating and the incident and scattered waves is shown in Fig. 1. We focus on arrays of periodically placed clusters with the intent of using the cluster properties to control forward and backward scattering. Our approach is to first generalize the forward-scattering methods of Evans and Porter [9] and Torrent *et al.* [11]. The derived expressions are then used to set up and solve the inverse grating problem. Most importantly, we note that Torrent *et al.* [11] first presented a formalism for dealing with periodically arranged clusters of scatterers. This approach is the basis for the present work.

The paper is organized as follows: In Sec. II we formulate the diffraction problem of a flexural plane wave by a periodic arrangement of clusters of  $N$  scatterers. In Sec. III we define the inverse grating problem and show its solution, and in Sec. IV we apply the theory to the design of a negative refractor. Finally, Sec. VI summarizes the work. Some mathematical results are derived in the Appendixes A and B.

## II. DIFFRACTION BY A PERIODIC ARRANGEMENT OF POINT SCATTERERS

### A. Scattering by a single point impedance and a cluster of point impedances

The deflection  $w(\mathbf{r})$  on a two-dimensional plate,  $\mathbf{r} = x\hat{\mathbf{x}} + y\hat{\mathbf{y}}$ , satisfies the Kirchhoff plate equation

$$D[\Delta^2 w(\mathbf{r}) - k^4 w(\mathbf{r})] = 0, \quad (1)$$

where  $k^4 = \rho h \omega^2 / D$ ,  $D$  is the bending stiffness,  $h$  is the plate thickness, and  $\rho$  is the density. Time-harmonic dependence  $e^{-i\omega t}$  is assumed. Equation (1) holds everywhere on the infinite plate except where there are point impedances attached [9].

Consider first scattering from a single point attachment located at  $\mathbf{r} = \mathbf{R}$ :

$$D[\Delta^2 w(\mathbf{r}) - k^4 w(\mathbf{r})] = \mu w(\mathbf{R}) \delta(\mathbf{r} - \mathbf{R}). \quad (2)$$

The attached-oscillator impedance  $\mu$  is modeled as a single degree of freedom with mass  $M$ , spring stiffness  $\kappa$ , and damping coefficient  $\nu$ . Two possible models are

$$\mu = \begin{cases} \left( \frac{1}{M\omega^2} - \frac{1}{\kappa - i\omega\nu} \right)^{-1} & \text{(model a),} \\ M\omega^2 - \kappa + i\omega\nu & \text{(model b).} \end{cases} \quad (3)$$

In model *a*, the mass is attached to the plate by a spring and damper acting in parallel [11]. Model *b* assumes the mass is rigidly attached to the plate, and both are attached to a rigid foundation by the spring and damper in parallel [9]. An important limit is a pointwise pinned plate,  $w(\mathbf{R}) = 0$ , which corresponds to  $\mu \rightarrow \infty$ . The point attachments considered here are based on devices proposed for passive control of flexural waves using *tuned vibration absorbers* (TVAs) [22–24]. A TVA, modeled as a point translational impedance, can be used to reduce vibration at a specific frequency or to control transmission and reflection of flexural waves in a beam [23,24]. The alternative term ‘‘vibration neutralizer’’ [22] is sometimes used. In the present context, the point impedance, or TVA, is considered as a device for controlling the scattering of flexural waves in a two-dimensional setting rather than in a one-dimensional setting.

The total plate deflection is

$$w(\mathbf{r}) = w_{\text{in}}(\mathbf{r}) + BG(\mathbf{r} - \mathbf{R}), \quad (4)$$

where  $w_{\text{in}}(\mathbf{r})$  is the incident field and, by definition of the point impedance,

$$B = \mu w(\mathbf{R}). \quad (5)$$

Also,  $G$  is the Green’s function (see Appendix A)

$$G(\mathbf{r}) = C[H_0^{(1)}(kr) - H_0^{(1)}(ikr)], \quad (6)$$

where  $C = G(\mathbf{0}) = i/(8k^2 D)$ . Note that  $H_0^{(1)}(ikr) = -(2i/\pi)K_0(kr)$ . Setting  $\mathbf{r} = \mathbf{R}$  in Eq. (4) and using Eq. (5), we obtain

$$B = \frac{w_{\text{in}}(\mathbf{R})}{\mu^{-1} - G(\mathbf{0})}. \quad (7)$$

If there are  $N$  point scatterers located at  $\mathbf{R}_\alpha = x_\alpha \hat{\mathbf{x}} + y_\alpha \hat{\mathbf{y}}$  with impedances  $\mu_\alpha$ ,  $\alpha = 1, 2, \dots, N$ , then the total field

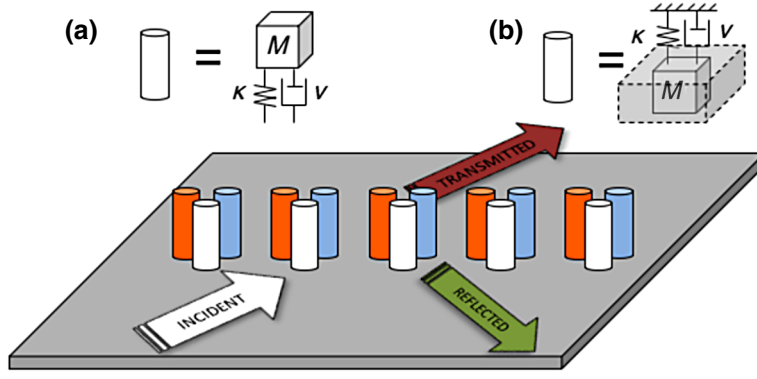


FIG. 1. The flexural wave grating problem: a line of clusters composed of multiple scatterers with possibly different mass, stiffness, and damping properties within the cluster (but the same for each cluster). Each scatterer can be modeled as an attached mass-spring-dashpot system with properly tuned constants  $M$ ,  $\kappa$ , and  $\nu$ . The schematic shows impedance models a and b in Eq. (3).

satisfies

$$D[\Delta^2 w(\mathbf{r}) - k^4 w(\mathbf{r})] = \sum_{\alpha=1}^N \mu_{\alpha} w(\mathbf{R}_{\alpha}) \delta(\mathbf{r} - \mathbf{R}_{\alpha}). \quad (8)$$

The solution is given by the incident field plus the field scattered by all the particles:

$$w(\mathbf{r}) = w_{\text{in}}(\mathbf{r}) + \sum_{\beta=1}^N B_{\beta} G(\mathbf{r} - \mathbf{R}_{\beta}), \quad B_{\beta} = \mu_{\beta} w(\mathbf{R}_{\beta}). \quad (9)$$

Our setting  $\mathbf{r} = \mathbf{R}_{\alpha}$  in Eq. (9) gives a linear system of  $N$  equations for the amplitudes:

$$\sum_{\beta=1}^N [\mu_{\alpha}^{-1} \delta_{\alpha\beta} - G(\mathbf{R}_{\alpha} - \mathbf{R}_{\beta})] B_{\beta} = w_{\text{in}}(\mathbf{R}_{\alpha}). \quad (10)$$

### B. Scattering by an infinite set of impedance clusters

The above set of equations provides the solution for the multiple-scattering problem of a given incident field on a cluster of small particles once their position and their physical nature are properly described. We wish to know what happens when this cluster is copied and distributed along a line and when the incident field is a plane wave of definite wavevector  $\mathbf{k}$ :

$$w_{\text{in}}(\mathbf{r}) = e^{i\mathbf{k}\cdot\mathbf{r}}. \quad (11)$$

This defines the grating scattering problem.

Specifically, the grating particle positions are

$$\mathbf{R}_{\beta m} = \mathbf{R}_{\beta} + \mathbf{R}_m, \quad (12)$$

where  $\beta = 1, 2, \dots, N$  defines the cluster element and  $\mathbf{R}_m = m\mathbf{a}$ ,  $m \in \mathbb{Z}$ , covers the infinite periodic grating. The

total field is then

$$w(\mathbf{r}) = w_{\text{in}}(\mathbf{r}) + \sum_{\beta=1}^N \sum_{\mathbf{R}_m} \mu_{\beta} w(\mathbf{R}_{\beta m}) G(\mathbf{r} - \mathbf{R}_{\beta m}). \quad (13)$$

It is assumed that the cluster-to-cluster relation for the total field satisfies the same phase relation as the incident field:

$$w(\mathbf{R}_{\beta m}) = w(\mathbf{R}_{\beta}) e^{i\mathbf{k}\cdot\mathbf{R}_m}. \quad (14)$$

This crucial identity implies that the total field can be represented in terms of  $N$  amplitudes,  $B_{\beta}$ ,  $\beta = \{1, 2, \dots, N\}$ :

$$w(\mathbf{r}) = e^{i\mathbf{k}\cdot\mathbf{r}} + \sum_{\beta=1}^N B_{\beta} \sum_{\mathbf{R}_m} e^{i\mathbf{k}\cdot\mathbf{R}_m} G(\mathbf{r} - \mathbf{R}_{\beta} - \mathbf{R}_m). \quad (15)$$

The amplitudes can be found by the same method as for the single cluster. Thus, our setting  $\mathbf{r} = \mathbf{R}_{\alpha}$  in Eq. (15) gives a linear system of  $N$  equations:

$$\sum_{\beta=1}^N (\mu_{\alpha}^{-1} \delta_{\alpha\beta} - \chi_{\alpha\beta}) B_{\beta} = e^{i\mathbf{k}\cdot\mathbf{R}_{\alpha}}, \quad (16)$$

with

$$\chi_{\alpha\beta} = \sum_{\mathbf{R}_m} e^{i\mathbf{k}\cdot\mathbf{R}_m} G(\mathbf{R}_{\alpha} - \mathbf{R}_{\beta} - \mathbf{R}_m). \quad (17)$$

### C. Solution of the forward-scattering grating problem

The  $N$  cluster repeats along a line,

$$\mathbf{R}_m = m\mathbf{a}\hat{\mathbf{x}}, \quad m \in \mathbb{Z}, \quad (18)$$

and therefore we can use the lattice-sum identity (see Appendix A):

$$\sum_{\mathbf{R}_m} e^{i\mathbf{k}\cdot\mathbf{R}_m} G(\mathbf{r} - \mathbf{R}_m) = G_0 \sum_{n \in \mathbb{Z}} e^{i(k_x + g_n)x} \times \left( \frac{e^{-\zeta_- |y|}}{\zeta_-} - \frac{e^{-\zeta_+ |y|}}{\zeta_+} \right), \quad (19)$$

where  $G_0 = \frac{1}{4Dk^2a}$ ,  $g_n = \frac{2\pi}{a}n$ , and  $\zeta_{\pm} = [(k_x + g_n)^2 \pm k^2]^{1/2}$ , where  $\text{Im}\zeta_- \leq 0$ . Specifically, Eq. (19) implies that the total field (15) is

$$w(\mathbf{r}) = e^{i\mathbf{k}\cdot\mathbf{r}} + G_0 \sum_{\beta=1}^N B_{\beta} \sum_{n \in \mathbb{Z}} e^{i(k_x + g_n)(x - x_{\beta})} \times \left( \frac{e^{-\zeta_- |y - y_{\beta}|}}{\zeta_-} - \frac{e^{-\zeta_+ |y - y_{\beta}|}}{\zeta_+} \right), \quad (20)$$

where the  $N$  coefficients  $B_{\beta}$  follow from Eqs. (16) and (17) with [instead of the general form (10)]

$$\chi_{\alpha\beta} = G_0 \sum_{n \in \mathbb{Z}} e^{i(k_x + g_n)(x_{\alpha} - x_{\beta})} \left( \frac{e^{-\zeta_- |y_{\alpha} - y_{\beta}|}}{\zeta_-} - \frac{e^{-\zeta_+ |y_{\alpha} - y_{\beta}|}}{\zeta_+} \right). \quad (21)$$

This provides a much-more-computationally-efficient expression than the slowly convergent Eq. (17). Note that the semianalytical form for  $\chi_{\alpha\beta}$  is a consequence of the fact that the Green's function can be expressed as a Fourier integral. This indicates that the same procedure used in Appendix A would apply to other wave systems for which the Green's function does not have a closed-form solution.

The  $\zeta_+$  terms in the total field (20) all decay exponentially away from the line, while the  $\zeta_-$  terms also decay except for those for which  $\zeta_-$  is imaginary. The latter define the finite set of *propagating modes*,  $\mathbb{P}$  with  $N_P$  elements, defined as

$$\mathbb{P} = \{n \in \mathbb{Z} : |k_x + g_n| < k\}. \quad (22)$$

These are the values for which  $\zeta_-$  is purely (negative) imaginary and they correspond to the far-field diffraction orders of the grating; all others are strictly near field. Note that  $\mathbb{P}$  always includes the value  $n = 0$ , so  $N_P \geq 1$ .

Let  $\theta_0 \in [0, \pi/2]$  be the angle of incidence relative to the grating direction, so

$$\mathbf{k} = k_x \hat{\mathbf{x}} + k_y \hat{\mathbf{y}} = k \cos \theta_0 \hat{\mathbf{x}} + k \sin \theta_0 \hat{\mathbf{y}}. \quad (23)$$

In particular,  $k_x = k \cos \theta_0$  implies that the direction of the propagating mode  $n$  is defined by the angle

$$\theta_n = \cos^{-1} \left( \cos \theta_0 + \frac{2\pi}{ka} n \right), \quad \theta_n \in (0, \pi), \quad n \in \mathbb{P}. \quad (24)$$

Hence,  $\mathbb{P}$  can be considered as the set of  $n$  for which  $\theta_n$  is real valued. The far-field diffracted displacement is

$$w(\mathbf{r}) = e^{i\mathbf{k}\cdot\mathbf{r}} + \frac{iG_0}{k} \sum_{\beta=1}^N B_{\beta} \sum_{n \in \mathbb{P}} \frac{1}{\sin \theta_n} e^{ik[(x - x_{\beta}) \cos \theta_n + |y - y_{\beta}| \sin \theta_n]}, \quad |y| \rightarrow \infty. \quad (25)$$

The individual diffracted modes are therefore

$$w(\mathbf{r}) = \begin{cases} \sum_{n \in \mathbb{P}} t_n e^{i\mathbf{k}_n^+ \cdot \mathbf{x}}, & y \rightarrow \infty, \\ \sum_{n \in \mathbb{P}} r_n e^{i\mathbf{k}_n^- \cdot \mathbf{x}}, & y \rightarrow -\infty, \end{cases} \quad (26)$$

where  $\mathbf{k}_n^+$  and  $\mathbf{k}_n^-$  are the wavenumbers of the transmitted and reflected waves, respectively,

$$\mathbf{k}_n^{\pm} = k \cos \theta_n \hat{\mathbf{x}} \pm k \sin \theta_n \hat{\mathbf{y}}, \quad n \in \mathbb{P}, \quad (27)$$

and the  $2N_P$  transmission and reflection coefficients follow from Eqs. (25) and (26) as

$$\left. \begin{matrix} t_n - \delta_{n0} \\ r_n \end{matrix} \right\} = \frac{iG_0}{k \sin \theta_n} \sum_{\beta=1}^N B_{\beta} \times \begin{cases} e^{-i\mathbf{k}_n^+ \cdot \mathbf{R}_{\beta}}, \\ e^{-i\mathbf{k}_n^- \cdot \mathbf{R}_{\beta}}, \end{cases} \quad n \in \mathbb{P}. \quad (28)$$

Note that  $\mathbf{k}_0^+ = \mathbf{k}$ , the incident wavevector, and that conservation of energy requires

$$\sum_{n \in \mathbb{P}} (|r_n|^2 + |t_n|^2) \sin \theta_n \leq \sin \theta_0 \quad (29)$$

with equality if the impedances  $\mu_{\alpha}$  are all real valued (no damping).

Finally, we note that if all the scatterers lie along a line parallel to the  $x$  axis (i.e.,  $y_{\beta} = b$  for all  $\beta$  for some  $b$ ), then

$$t_n - \delta_{n0} = r_n e^{-i2kb \sin \theta_n}, \quad n \in \mathbb{P}. \quad (30)$$

The number of independent scattering coefficients is therefore greatly reduced. This redundancy has implications in the selection of scatterer positions for the inverse grating problem, which is considered next.

### III. THE INVERSE GRATING PROBLEM

We are interested in controlling the reflection and transmission coefficients through (inverse) design of the grating. For instance, Fig. 2 shows a grating that makes all but one of the scattered modes vanish; in this case all except the  $n = -1$  mode. Specific designs for this type of grating are given below. The design and control is achieved with use of the combined degrees of freedom of the cluster spatial distribution,  $\mathbf{R}_m$ , the scatterers' positions,  $\mathbf{R}_{\alpha}$ , and their impedances,  $\mu_{\alpha}$ . We consider the incident direction  $\theta_0$  and the nondimensional frequency  $ka$  as given quantities. The inverse problem as posed is still highly nonunique since there could be multiple configurations that achieve the same objective. We therefore concentrate on specific geometrical configurations for the cluster distributions, such as a cluster of  $N = 3$  scatterers positioned at the vertices of a triangle or along a line. This allows us to focus on the inverse problem of finding the impedances, and specifically on making them passive but with as little damping as possible so that all of the incident energy is channeled into the selected-mode diffraction.

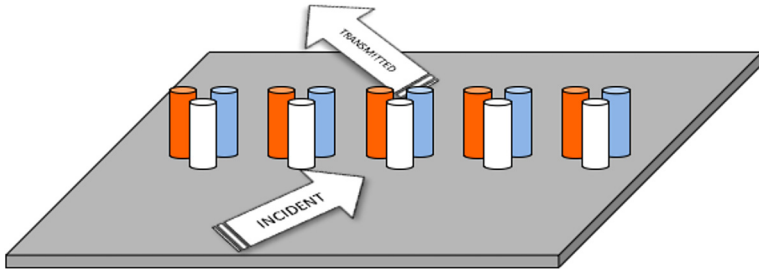


FIG. 2. A grating that channels all of the wave energy into the  $n = -1$  diffracted mode.

### A. Inverting for impedances

Equation (16) written in matrix form is

$$\mathbf{E} = \mathbf{M}\mathbf{B}, \quad (31)$$

where the  $N \times N$  matrix  $\mathbf{M}$  follows from Eq. (16) and the  $N$ -vector  $\mathbf{E}$  contains the incident-wave amplitudes at the  $N$  scatterer positions:

$$\mathbf{M} = \boldsymbol{\mu}^{-1} - \boldsymbol{\chi}, \quad \boldsymbol{\mu} = \begin{pmatrix} \mu_1 & & & 0 \\ & \mu_2 & & \\ & & \ddots & \\ 0 & & & \mu_N \end{pmatrix}, \quad (32)$$

$$\mathbf{E} = \begin{pmatrix} e^{i\mathbf{k}\cdot\mathbf{R}_1} \\ e^{i\mathbf{k}\cdot\mathbf{R}_2} \\ \vdots \\ e^{i\mathbf{k}\cdot\mathbf{R}_N} \end{pmatrix}.$$

The elements of the  $N \times N$  matrix  $\boldsymbol{\chi}$  are defined by the infinite sums (20). Using the fact that  $\boldsymbol{\mu}$  is diagonal, we can reconsider Eq. (31) as an equation for  $\boldsymbol{\mu}$  in terms of the amplitudes  $B_\alpha$ :

$$\mu_\alpha^{-1} = (e^{i\mathbf{k}\cdot\mathbf{R}_\alpha} + \mathbf{e}_\alpha^T \boldsymbol{\chi} \mathbf{B}) / B_\alpha, \quad (33)$$

where the elements of the  $N$ -vector  $\mathbf{e}_\alpha$  are zero except for the  $\alpha$ th, which is unity. To proceed we need to obtain the amplitudes  $\mathbf{B}$ .

The goal is to control transmission coefficients, so we therefore collect the transmission and reflection coefficients into a  $2N_P$ -vector denoted by  $\mathbf{T} = [(t_n - \delta_{n0})(\sin \theta_n / \sin \theta_0), r_n(\sin \theta_n / \sin \theta_0)]^T$  with  $n \in \mathbb{P}$ . The vector length,  $2N_P$ , depends on the number of diffraction orders. We may rewrite the equations for the transmission and reflection coefficients, Eq. (28), as

$$\mathbf{T} = \mathbf{S}\mathbf{B}, \quad (34)$$

with  $\mathbf{S}$ , a  $2N_P \times N$  matrix, collecting the exponential terms related to scatterer positions:

$$\mathbf{S} = \frac{iG_0}{k \sin \theta_0} \begin{pmatrix} e^{-i\mathbf{k}_0^+ \cdot \mathbf{R}_1} & e^{-i\mathbf{k}_0^+ \cdot \mathbf{R}_2} & \dots & e^{-i\mathbf{k}_0^+ \cdot \mathbf{R}_N} \\ e^{-i\mathbf{k}_0^- \cdot \mathbf{R}_1} & e^{-i\mathbf{k}_0^- \cdot \mathbf{R}_2} & \dots & e^{-i\mathbf{k}_0^- \cdot \mathbf{R}_N} \\ e^{-i\mathbf{k}_{-1}^+ \cdot \mathbf{R}_1} & e^{-i\mathbf{k}_{-1}^+ \cdot \mathbf{R}_2} & \dots & e^{-i\mathbf{k}_{-1}^+ \cdot \mathbf{R}_N} \\ e^{-i\mathbf{k}_{-1}^- \cdot \mathbf{R}_1} & e^{-i\mathbf{k}_{-1}^- \cdot \mathbf{R}_2} & \dots & e^{-i\mathbf{k}_{-1}^- \cdot \mathbf{R}_N} \\ \vdots & \vdots & \vdots & \vdots \\ e^{-i\mathbf{k}_{n_P}^+ \cdot \mathbf{R}_1} & e^{-i\mathbf{k}_{n_P}^+ \cdot \mathbf{R}_2} & \dots & e^{-i\mathbf{k}_{n_P}^+ \cdot \mathbf{R}_N} \\ e^{-i\mathbf{k}_{n_P}^- \cdot \mathbf{R}_1} & e^{-i\mathbf{k}_{n_P}^- \cdot \mathbf{R}_2} & \dots & e^{-i\mathbf{k}_{n_P}^- \cdot \mathbf{R}_N} \end{pmatrix}, \quad (35)$$

where  $n_P$  indicates the  $N_P$ th diffracted mode.

We focus on the inverse grating problem of eliminating all but one of the  $2N_P$  transmission and reflection coefficients. Suppose we want all coefficients to vanish except, for instance,  $t_m$  or  $r_m$ ; then Eq. (34) provides  $2N_P - 1$  identities. To have a solvable linear but not overdetermined system we require that the number of unknowns equals the number of knowns, implying a relation between the number of scatterers and the number of diffracted modes:

$$N = 2N_P - 1. \quad (36)$$

The magnitude of the remaining coefficient must satisfy Eq. (29), implying

$$\hat{\mathbf{T}} = \hat{\mathbf{S}}\mathbf{B}, \quad (37)$$

where the  $N$ -vector  $\hat{\mathbf{T}}$  ( $N = 2N_P - 1$  vector) follows from  $\mathbf{T}$  by removal of the row for  $t_m$  or  $r_m$ , and the square  $N \times N$  matrix  $\hat{\mathbf{S}}$  is obtained from the  $2N_P \times 2N_P - 1$  matrix  $\mathbf{S}$  by removal of the row corresponding to the unconstrained coefficient ( $t_m$  or  $r_m$ ). The  $N$ -scatterer amplitudes are therefore

$$\mathbf{B} = \hat{\mathbf{S}}^{-1} \hat{\mathbf{T}}. \quad (38)$$

It is important to note that we are assuming a nonsingular  $\hat{\mathbf{S}}$ ; the possibility and implications of  $\hat{\mathbf{S}}$  being singular are discussed later. Substitution of  $\mathbf{B}$  into (33) yields the

impedances in terms of the transmission/reflection vector  $\hat{\mathbf{T}}$  as

$$\mu_\alpha^{-1} = \frac{e^{ik \cdot \mathbf{R}_\alpha} + \mathbf{e}_\alpha^T \boldsymbol{\chi} \hat{\mathbf{S}}^{-1} \hat{\mathbf{T}}}{\mathbf{e}_\alpha^T \hat{\mathbf{S}}^{-1} \hat{\mathbf{T}}}, \quad \alpha = 1, 2, \dots, N. \quad (39)$$

Equation (39) provides a simple inversion procedure at a given frequency for a given arrangement of scatterers, the number of which,  $N$ , is related to the number of diffraction orders,  $N_P$ , by Eq. (36). The latter implies that the number of scatterers is *odd*. The solution [Eq. (39)] yields complex values for the impedances. A realistic solution requires the further condition that the impedances are passive, which is the case only if  $\text{Im}\mu_\alpha \geq 0$  ( $\text{Im}\mu_\alpha^{-1} \leq 0$ ) for all  $\alpha = 1, 2, \dots, N$ .

An explicit solution follows for the case in which all coefficients vanish except for the fundamental transmission  $t_0$ . Then  $\hat{\mathbf{T}} = \mathbf{0}$ , implying, from Eq. (39), that  $\mu_\alpha = 0$ . The solution is trivial: there is no grating. For every other case, no matter which of the remaining  $N = 2N_P - 1$  coefficients is chosen as the one that is nonzero, the  $N$ -vector  $\hat{\mathbf{T}}$  has the same form:

$$\hat{\mathbf{T}} = (-1, 0, 0, \dots, 0) = -\mathbf{e}_1. \quad (40)$$

Equation (39) therefore simplifies to

$$\mu_\alpha^{-1} = \frac{\mathbf{e}_\alpha^T \boldsymbol{\chi} \hat{\mathbf{S}}^{-1} \mathbf{e}_1 - e^{ik \cdot \mathbf{R}_\alpha}}{\mathbf{e}_\alpha^T \hat{\mathbf{S}}^{-1} \mathbf{e}_1}, \quad \alpha = 1, 2, \dots, N. \quad (41)$$

In summary, if the impedances satisfy Eq. (41) then all but one of the transmission and reflection coefficients vanish.

The matrix  $\hat{\mathbf{S}}$  is invertible if and only if it is full rank (i.e., with  $N$  linearly independent rows). If the scatterers are positioned along a line parallel to the  $x$  axis at the common coordinate  $y_\beta = b$ , then with reference to

Eq. (35),  $e^{-ik_n^+ \cdot \mathbf{R}_\alpha} = e^{-ik_n^- \cdot \mathbf{R}_\alpha} e^{-i2kb \sin \theta_n}$ . This implies that  $\hat{\mathbf{S}}$  has at most  $(N - 1)/2$  linearly dependent rows, and therefore the rank of the matrix falls precipitously from  $N$  to  $\frac{1}{2}(N + 1) = N_P$ ; see Eq. (36). Despite this singularity, it may happen that Eq. (41) has a finite value by virtue of it containing  $\hat{\mathbf{S}}^{-1} \mathbf{e}_1$  in the numerator and in the denominator. Also,  $\hat{\mathbf{S}}^{-1} \mathbf{e}_1$  itself can be finite even though  $\hat{\mathbf{S}}$  is singular, as is the case in the example in Appendix B. Finally, the obvious exception to this discussion is the simplest,  $N = 1$ , which is considered next.

#### IV. EXAMPLES AND APPLICATIONS

Following the theoretical developments for the inverse design of gratings outlined in Sec. III, we now present and discuss examples and applications. We first focus on the simple case of  $N = 1$ , when only one diffracted mode exists; that is,  $n \in \mathbb{P} = \{0\}$ . A more-complex design for  $N = 3$  (with  $\mathbb{P} = \{-1; 0\}$ ) is then developed with particular focus on the inverse design of the cluster. This configuration is used to find scatterer configurations resulting in the negative refraction of waves at the grating.

The negative refractor consists of a grating that diverts an incoming wave in such a way that if the angle the wave makes with the  $x$  axis is  $\theta_0$ , that of the transmitted wave is  $\pi - \theta_0$ . This is indeed the “refraction” version of the retroreflector, in which the incident wave is retroreflected. From the diffraction point of view we assume that the selected angle of incidence  $\theta_0$  allows two diffracted modes  $\mathbb{P} = \{-1; 0\}$ . We also want the angle of the  $n = -1$  mode to be  $\theta_n = \pi - \theta_0$ ; therefore, with  $k = 2\pi/\lambda$  Eq. (24) gives

$$-\cos \theta_0 = \cos \theta_0 - \frac{\lambda}{a}, \quad (42)$$

which sets up the ratio  $\lambda/a = 2 \cos \theta_0$  (or  $ka = \pi \sec \theta_0$ ). A configuration of  $N = 3$  scatterers is used to demonstrate the negative refractor.

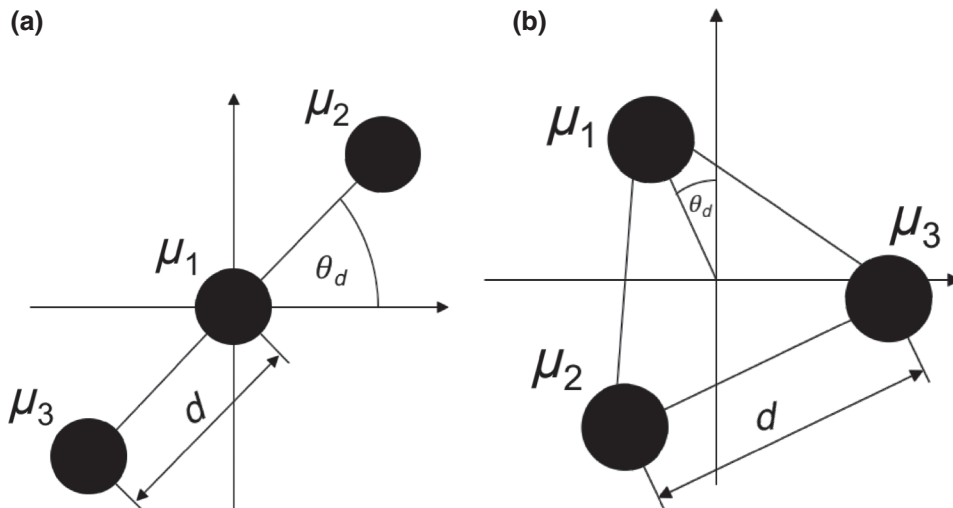


FIG. 3. Two investigated cluster configurations: linear (left) and triangular (right).

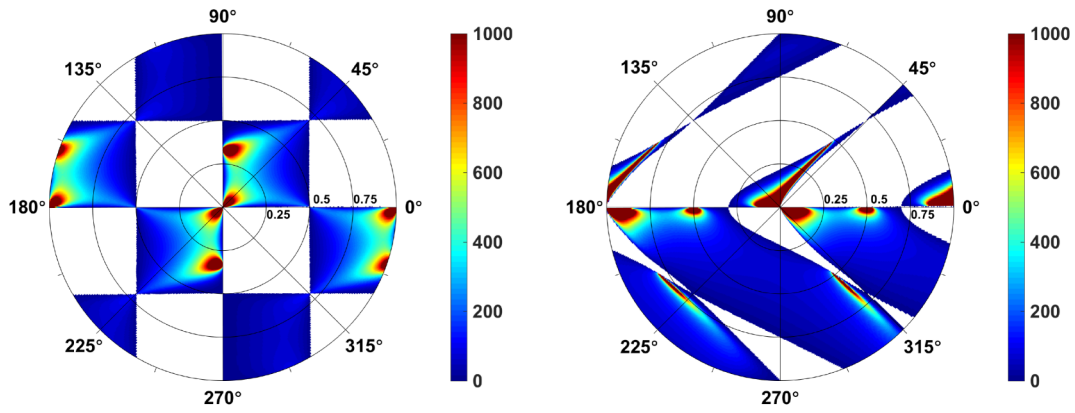


FIG. 4. Imaginary parts of the complex-valued impedance  $\mu_1$  (left) and  $\mu_2$  (right) in the unit of  $a^2/D$  as functions of  $d$  and  $\theta_d$  for a fixed incident-wavevector angle  $\theta_0 = \pi/4$  and  $k = \pi/(a \cos \theta_0)$  (for  $a = 1$ ) for the  $N = 3$  linear-cluster negative refractor. The plot shows only regions for which the impedances are passive:  $\text{Im}\mu_1, \mu_2 \geq 0$ .

### A. The simple grating: $N = 1$

By assumption, the fundamental is the only diffracted order and the only transmission/reflection coefficients are related by  $t_0 = r_0 + 1$ , assuming with no loss in generality that it is positioned at  $\mathbf{R}_1 = \mathbf{0}$ . Equation (41), the condition for total reflection ( $t_0 = 0 \Rightarrow r_0 = -1$ ), reduces to a scalar relation:

$$\mu^{-1} = \chi - \frac{iG_0}{k \sin \theta_0}, \quad (43)$$

where  $\chi = \chi_{\alpha\alpha}$  follows from Eq. (21). In particular [9], since  $\mathbb{P} = \{0\}$ ,

$$\begin{aligned} \chi - \frac{iG_0}{k \sin \theta_0} \equiv \chi_1 &= \frac{-G_0}{k\sqrt{1 + \cos^2 \theta_0}} \\ &+ G_0 \sum_{n \in \mathbb{Z} \setminus \{0\}} \left[ \frac{1}{\sqrt{(k_x + g_n)^2 - k^2}} - \frac{1}{\sqrt{(k_x + g_n)^2 + k^2}} \right], \end{aligned} \quad (44)$$

where  $\chi_1$  is real. Total reflection can therefore be achieved with real impedance  $\mu = \chi_1^{-1}$ , a result previously obtained in Ref. [9].

Since there is only one scattering coefficient in this case (because  $t_0 = r_0 + 1$ ), it is of interest to see what other values of  $t_0$  can be achieved. Instead of using Eq. (40), we retain  $t_0 \neq 0$  and set  $\hat{T} = t_0 - 1$ . Equation (39) then simplifies to

$$\mu^{-1} = \frac{iG_0 t_0}{k \sin \theta_0 (t_0 - 1)} + \chi_1. \quad (45)$$

Equation (45) provides an explicit expression for the impedance for a given incident direction  $\theta_0$ , lattice spacing  $a$ , wavenumber  $k$ , and transmission  $t_0$ . The impedance is complex valued, indicating damping is necessary, except for the two limiting values  $t_0 = 0$ , discussed above, and  $t_0 = 1$ , which is the trivial limit of  $\mu = 0$  (i.e., no grating).

What other values of  $t_0$  can be achieved with a *passive* impedance? Recall that a passive impedance maintains or dissipates energy, as opposed to an active

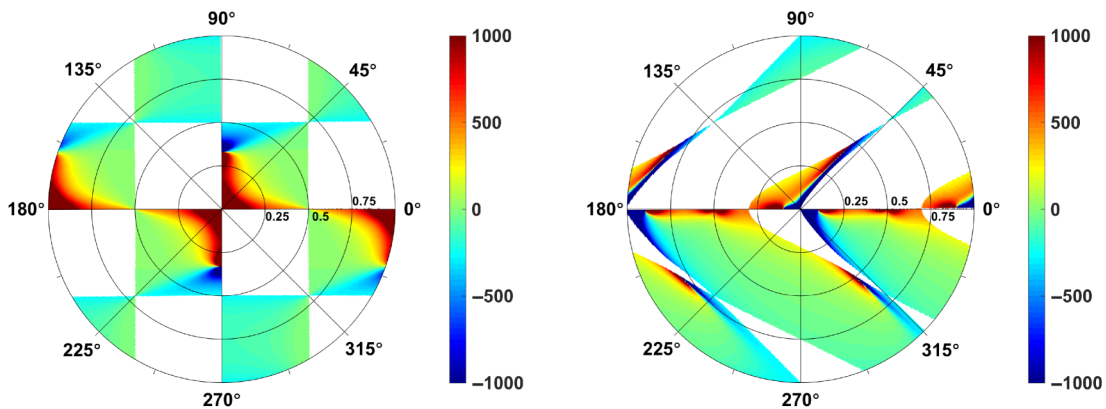


FIG. 5. Real parts of the impedances  $\mu_1$  (left) and  $\mu_2$  (right) in the unit of  $a^2/D$  as functions of  $d$  and  $\theta_d$  for incident-wavevector angle  $\theta_0 = \pi/4$  and  $k = \pi/(a \cos \theta_0)$  (for  $a = 1$ ) for the  $N = 3$  linear-cluster negative refractor. The plot is restricted to passive impedances; see Fig. 4.

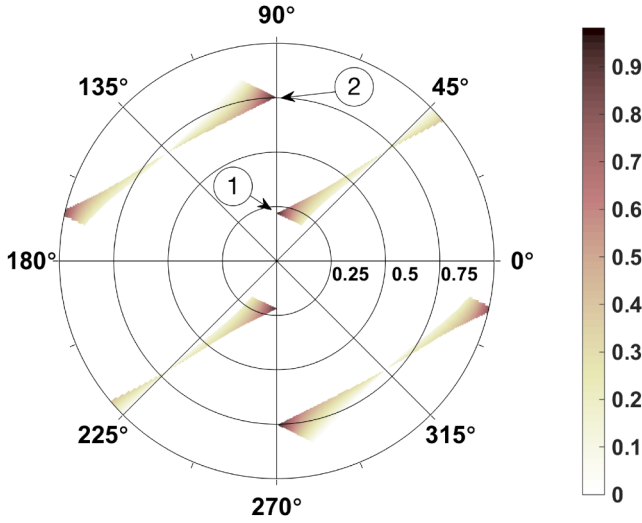


FIG. 6. Magnitude of the transmission coefficient  $t_{-1}$  for the designed linear three-cluster negative refractor as a function of  $(d, \theta_d)$  plotted in polar coordinates. The regions shown correspond to passive  $\mu_\alpha$  for all  $\alpha$ , and the labels on the selected points correspond to the clusters in Table I.

impedance, which requires an external energy source. The impedance is passive if and only if  $\text{Im}\mu^{-1} \leq 0$  [see, e.g., Eq. (3)]. Equation (45) gives a passive  $\mu$  if and only if  $\text{Re}[t_0/(t_0 - 1)] \leq 0$ . Hence,

$$t_0 = |t_0|e^{i\phi}, \quad |t_0| \leq \cos \phi \Leftrightarrow \text{passive } \mu. \quad (46)$$

In addition to the limits  $t_0 = 1$  and  $t_0 = 0$  discussed above, this provides the entire range of transmission coefficients achievable with  $N = 1$ .

### B. The next-simplest grating: $N = 3$

There are two diffracted modes,  $\mathbb{P} = \{-1; 0\}$ , if the angle of incidence  $\theta_0$  is large enough, which is now assumed. Following the discussion in Sec. III, we need three scatterers,  $N = 3$ , to control three of four reflection and transmission coefficients. With the goal of designing a negative refractor, we want the only propagating mode, among all modes transmitted through or reflected from the grating, to be the transmitted  $n = -1$  order. A grating that sends all of the incident energy into the transmitted  $n = -1$

mode has matrix  $\hat{S}$ :

$$\hat{S} = \frac{iG_0}{k \sin \theta_0} \begin{pmatrix} e^{-ik_0^+ \cdot \mathbf{R}_1} & e^{-ik_0^+ \cdot \mathbf{R}_2} & e^{-ik_0^+ \cdot \mathbf{R}_3} \\ e^{-ik_0^- \cdot \mathbf{R}_1} & e^{-ik_0^- \cdot \mathbf{R}_2} & e^{-ik_0^- \cdot \mathbf{R}_3} \\ e^{-ik_{-1}^- \cdot \mathbf{R}_1} & e^{-ik_{-1}^- \cdot \mathbf{R}_2} & e^{-ik_{-1}^- \cdot \mathbf{R}_3} \end{pmatrix}. \quad (47)$$

We consider two particular geometrical setups for  $N = 3$  clusters; namely, a linear cluster and a triangular cluster, as shown in Fig. 3. In each case we parametrize the cluster by the spacing between the scatterers and the rotation angle of the cluster,  $d$  and  $\theta_d$ , respectively. The positions of the scatterers in the cluster are then  $\mathbf{R}_1 = (0, 0)$  and  $\mathbf{R}_2 = \pm d(\cos \theta_d, \sin \theta_d)$ ,  $d > 0$ , for the linear cluster and  $\mathbf{R}_1 = d/\sqrt{3}(-\sin \theta_d, \cos \theta_d)$  and  $\mathbf{R}_3 = d/\sqrt{3}[\sin(\theta_d \mp \pi/6), -\cos(\theta_d \mp \pi/6)]$  for the triangular cluster.

The design process for a grating consists in finding the scatterers' impedances and positions  $(d, \theta_d)$ . Among all possible solutions, we are interested in passive cluster configurations, (i.e.,  $\text{Im}\mu_\alpha > 0$  for all  $\alpha$ ) that correspond to the largest-possible transmission coefficient  $|t_{-1}|$ . The latter would imply that possibly a large portion of the energy of the incident wave is sent into the transmitted  $n = -1$  mode, resulting in the negative refractor. From a practical perspective, a particularly interesting cluster setup would satisfy  $\text{Im}\mu_\alpha = 0$ , resulting in spring-mass configurations of the scatterers only (no damping).

In the following examples we assume the incident wavevector  $k = \pi/(a \cos \theta_0)$  at angle  $\theta_0 = \pi/4$ . In each case all but  $t_{-1}$  reflection and transmission coefficients in  $\hat{\mathbf{T}}$  are set to zero. We also assume, for simplicity,  $D = 1$  and  $a = 1$ .

## C. Numerical examples

### 1. Results for the linear cluster

We begin by inverting  $\hat{S}$  from Eq. (47) and using Eq. (39) to solve for impedances. Figures 4 and 5 show, respectively, the imaginary and real parts of the complex-valued impedance  $\mu_1$  and  $\mu_2$  ( $\mu_3$  is similar to  $\mu_2$  due to the symmetry of the cluster) for  $\theta_d \in (0, 2\pi)$  and  $d \in (0, a)$ . As we are interested in passive solutions only, the plots in Figs. 4 and 5 are limited to  $(d, \theta_d)$  combinations, resulting in  $\text{Im}\mu_\alpha > 0$  for respective scatterers independently. A cluster with passive damping properties can be constructed

TABLE I. Selected cluster configurations for  $N = 3$ ; see Fig. 3. The factor  $10^2$  applies to all values except those in the first row.

|                 | Linear cluster 1   | Linear cluster 2    | Triangular cluster 1 | Triangular cluster 2 |
|-----------------|--------------------|---------------------|----------------------|----------------------|
| $(d, \theta_d)$ | $(0.225, \pi/2)$   | $(0.751, \pi/2)$    | $(0.7484, 0.9237)$   | $(1.438, 1.281)$     |
| $\mu_1 a^2/D$   | $9.7253 + 0.2878i$ | $-1.2684 + 0.0095i$ | $-1.8861 + 0.0141i$  | $-3.4707 + 0.1240i$  |
| $\mu_2 a^2/D$   | $2.2272 + 0.0022i$ | $-0.8477 + 0.0043i$ | $-0.6507 + 0.5238i$  | $-4.0771 + 0.0308i$  |
| $\mu_3 a^2/D$   | $2.1609 + 0.0370i$ | $-0.8308 + 0.0120i$ | $1.5165 + 0.0588i$   | $-0.4929 + 0.3752i$  |



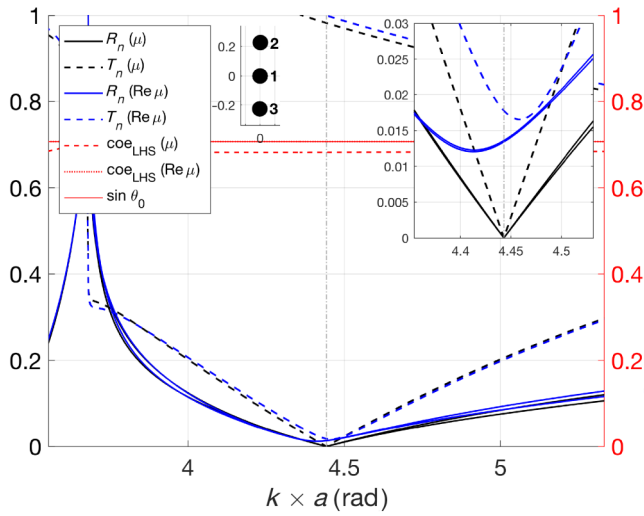


FIG. 7. Reflection and transmission coefficients for linear cluster 1 computed for impedances given in Table I for complex values of  $\mu_\alpha$  and for  $\text{Im}\mu_\alpha = 0$ . The vertical dash-dotted line at  $k \times a = \pi / \cos \pi/4$  indicates the operating frequency of the grating. coe, coefficient; LHS, left-hand side.

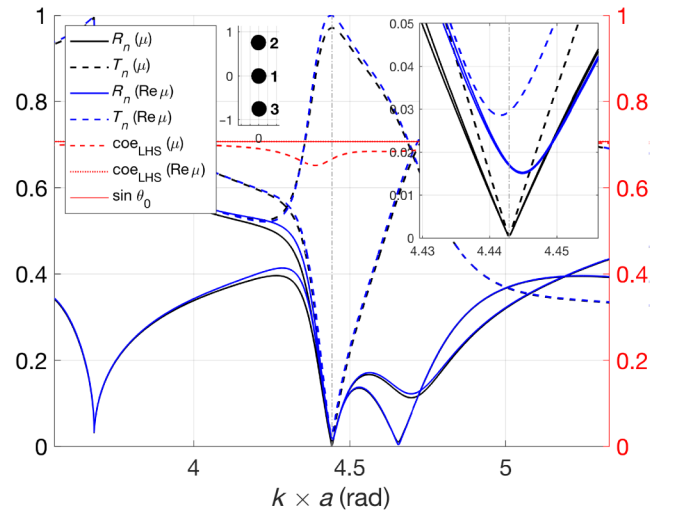


FIG. 8. Reflection and transmission coefficients for linear cluster 2 computed with impedances from Table I for complex values of  $\mu_\alpha$  and for  $\text{Im}\mu_\alpha = 0$ . The vertical dash-dotted line at  $k \times a = \pi / \cos \pi/4$  indicates the operating frequency of the grating. coe, coefficient; LHS, left-hand side.

only by selection of scatterers' positions corresponding to impedances satisfying  $\text{Im}\mu_\alpha > 0$  for all  $\alpha$ . Those combinations of  $(d, \theta_d)$  with the values of  $|t_{-1}|$  are shown in Fig. 6.

Cluster configurations corresponding to the highest values of  $|t_{-1}|$  are preferred. The largest values of  $|t_{-1}|$  in Fig. 6 are obtained for clusters oriented vertically. Figure 6 also indicates that zero-transmission points occur at cluster angles perpendicular or parallel to the incident wavefront. For detailed investigation we select  $(d, \theta_d)$  pairs with large values of  $|t_{-1}|$ ; namely,  $(0.225, \pi/2)$  and  $(0.751, \pi/2)$ . The corresponding impedances of the scatterers are listed in Table I. The two selected clusters differ only in the (vertical) spacing  $d$ , and the difference between the two values,  $d_2 - d_1 \approx 0.5$ , corresponds to a phase change of  $k_y(d_2 -$

$d_1) \approx \pi/2$ . Other points with the same high transmission correspond to  $2\pi$  phase change in the  $y$  direction, and are situated outside the region shown above (and below) clusters 1 and 2.

It might seem surprising that the optimal orientation of the linear cluster is vertical, since it is clear from Eq. (47) and the identities  $\mathbf{k}_{-1}^\pm = -\mathbf{k}_0^\mp$  for the negative refractor that if the three scatterers are on a line parallel to the  $y$  axis, then the second and third rows of  $\hat{\mathbf{S}}$  are identical, making the matrix singular. However, it is shown in Appendix B that even though the matrix  $\hat{\mathbf{S}}$  is indeed singular for  $\theta_d = \pi/2$ , the vector  $\hat{\mathbf{S}}^{-1} \mathbf{e}_1$  that appears in Eq. (41) remains finite. The symmetry of the three-cluster for  $\theta_d = \pi/2$  also

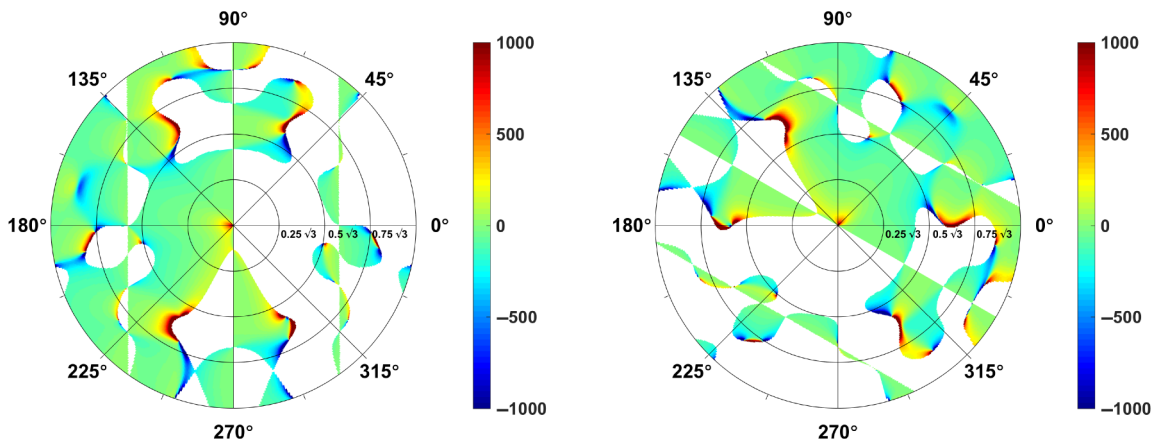


FIG. 9. Real parts of the complex-valued impedance  $\mu_1$  (left) and  $\mu_2$  (right) in the unit of  $a^2/D$  as functions of  $d$  and  $\theta_d$  for the incident wave  $\theta_0 = \pi/4$  and  $k = \pi/(a \cos \theta_0)$  (with  $a = 1$ ) for the  $N = 3$  triangular-cluster negative refractor.

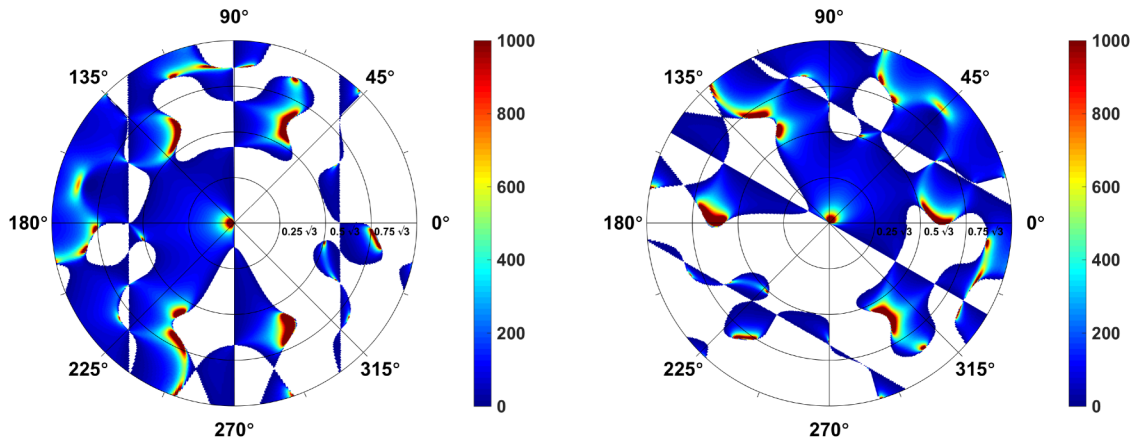


FIG. 10. Imaginary parts of the impedance  $\mu_1$  (left) and  $\mu_2$  (right) in the unit of  $a^2/D$  for the incident wave  $\theta_0 = \pi/4$ ,  $k = \pi/(a \cos \theta_0)$  (for  $a = 1$ ) for the  $N = 3$  triangular-cluster negative refractor.

implies that the matrix  $\chi$  in Eq. (17) is symmetric with only three independent elements, since  $\chi_{11} = \chi_{22} = \chi_{33}$  and  $\chi_{12} = \chi_{13}$ .

With use of impedances and cluster configurations from Table I, reflection and transmission coefficients and plate displacements at the scatterers are computed for a wide range of  $k \times a$ . Results for linear clusters 1 and 2 are shown in Figs. 7 and 8, respectively.

Horizontal continuous red lines in Figs. 7 and 8 (and later figures) define the energy-conservation threshold  $\sin \theta_0$  of Eq. (29), while the dotted red lines depict the energy associated with all propagation modes; that is, the left-hand side of Eq. (29). Conservation of energy requires

that the continuous line is above the dotted line, which is always the case in the examples considered.

Figures 7 and 8 illustrate relatively high transmission coefficients (approximately 0.97) for the  $n = -1$  diffracted mode for the linear clusters, meaning that almost all energy incident on the grating is converted to this mode. Of the two configurations, cluster 1 is more broadband (i.e., it achieves similar transmission properties for a wider range of  $k \times a$ ).

We next relax the restrictions on the impedances given in Table I by using only their real parts, with the results shown in Figs. 7 and 8 for linear clusters 1 and 2, respectively. It can be seen that for both clusters, the reflection and transmission coefficients of the diffracted

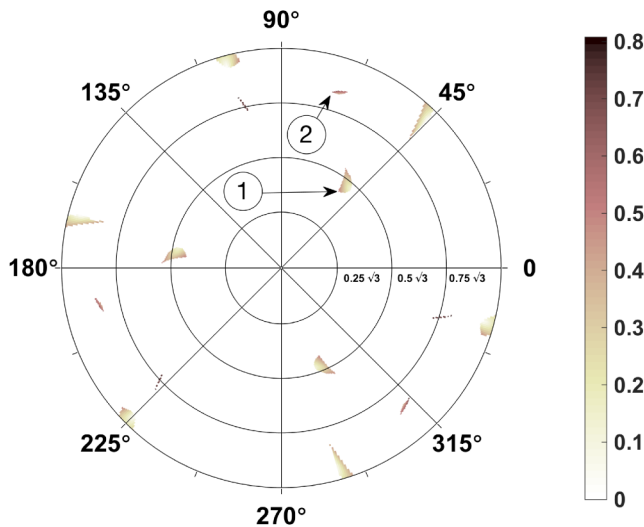


FIG. 11. Transmission magnitude  $|t_{-1}|$  of the designed triangular-cluster negative refractor as a function of the scatterers' radial,  $d$ , and angular,  $\theta_d$ , coordinates. The plotted regions correspond to passive  $\mu_\alpha$  for all  $\alpha$ , and the labels correspond to the selected clusters in Table I.

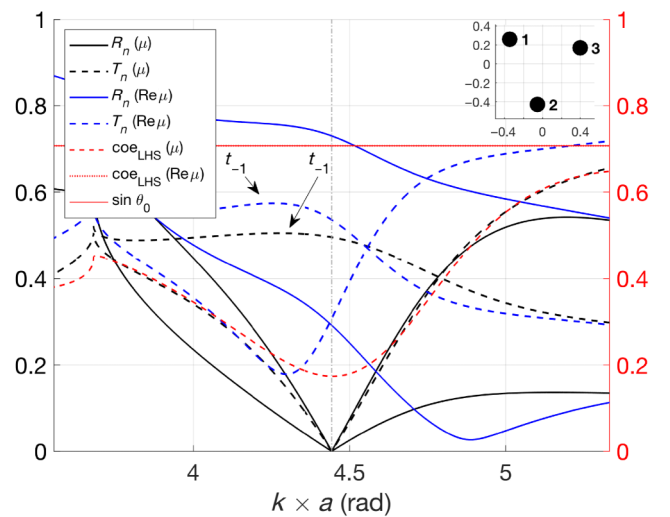


FIG. 12. Reflection and transmission magnitudes for triangular cluster 1 defined in Table I for complex values of  $\mu_\alpha$  and for  $\text{Im} \mu_\alpha = 0$ . The vertical dash-dotted line at  $k \times a = \pi/\cos \pi/4$  indicates the operating frequency. coe, coefficient; LHS, left-hand side.

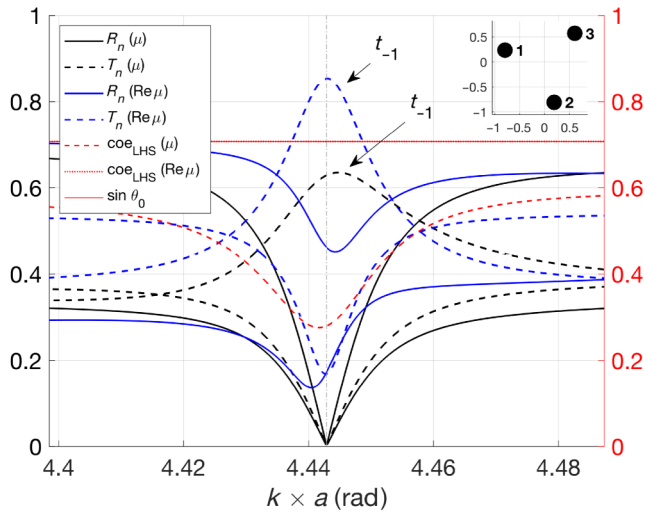


FIG. 13. Reflection and transmission magnitudes for triangular cluster 2 with properties from Table I for complex values of  $\mu_\alpha$  and for  $\text{Im}\mu_\alpha = 0$ . The vertical dash-dotted line at  $k \times a = \pi / \cos \pi/4$  indicates the operating frequency of the grating. coe, coefficient; LHS, left-hand side.

modes that were previously almost zero are now slightly increased; however, the target  $t_{-1}$  coefficient is still near unity (0.999). Also, cluster 1 displays better broadband

characteristics than cluster 2, the latter being more sensitive to precise selection of  $k$ . It is interesting to note that cluster 2 has small damping to begin with. Also, the real parts of the impedances in both clusters are all positive (cluster 1) or negative (cluster 2).

## 2. Results for the triangular cluster

Figures 9 and 10 show, respectively, real and imaginary parts of the complex-valued impedance  $\mu_1$  and (symmetric)  $\mu_2$  ( $\mu_3$  is also symmetric with respect to  $\mu_2$  due to the symmetry of the cluster) for  $\theta_d \in (0, 2\pi)$  and  $d \in (0, a)$  for the triangular cluster. Again, Figs. 9 and 10 only show the parts of the  $(d, \theta_d)$  plane for which  $\text{Im}\mu > 0$ . Combinations of  $(d, \theta_d)$  with the values of  $|t_{-1}|$  satisfying  $\text{Im}\mu_\alpha > 0$  for all  $\alpha$  (i.e., a passive cluster) are shown in Fig. 11.

As for the linear cluster, we select  $(d, \theta_d)$  pairs with relatively large values of  $|t_{-1}|$ . For the triangular cluster these are (0.7484, 0.9237) and (1.438, 1.281), with impedances listed in Table I. Figures 12 and 13 show the reflection and transmission coefficients as a function of  $k \times a$  for the chosen triangular clusters 1 and 2. Triangular cluster 1 displays a moderate broadband response, while the triangular cluster 2 exhibits a narrowband response, and thus sensitive to the frequency of the incident wave.

Figures 12 and 13 also show the reflection and transmission characteristics for triangular clusters 1 and 2,

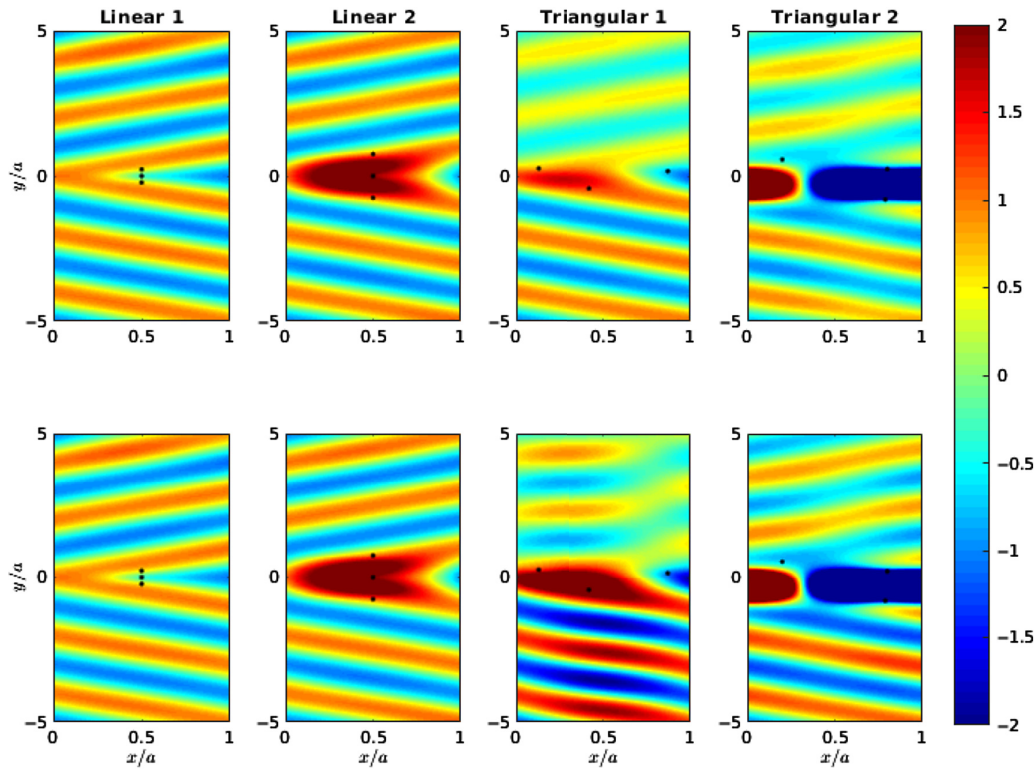


FIG. 14. Field maps of the diffraction of a plane wave by the different clusters of resonators as defined in Table I. The upper panels show the full solution and the lower panels show the same cluster but with  $\text{Im}\mu_\alpha = 0$ . The black dots represent the point impedances within one period of the infinite grating.

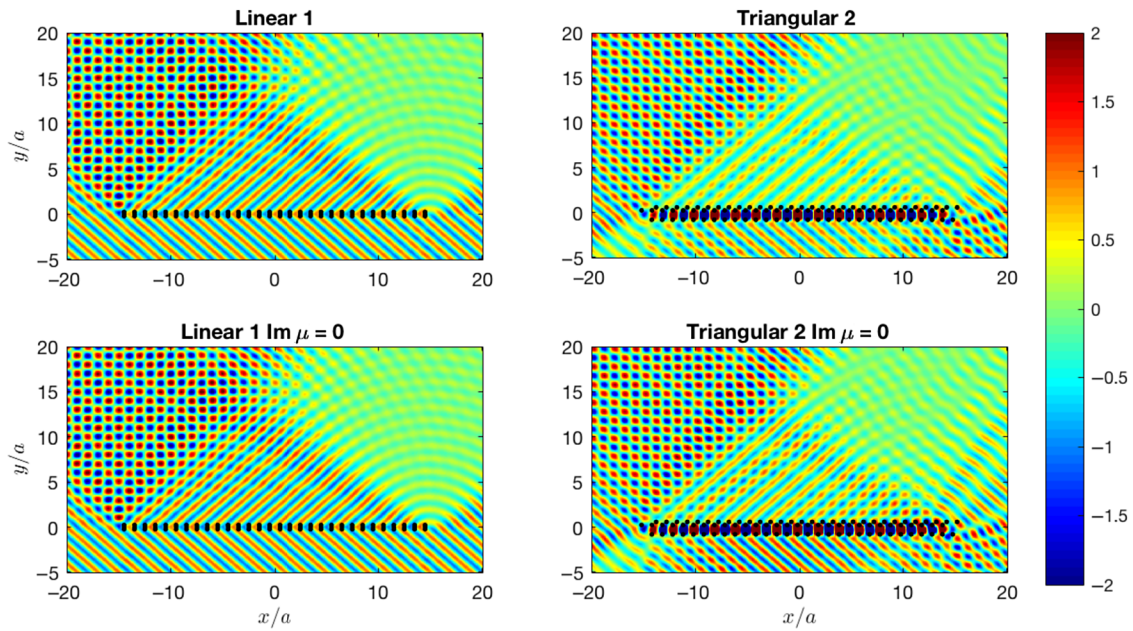


FIG. 15. The total field amplitude for plane-wave incidence on finite gratings of 30 clusters. The parameters are otherwise the same as in Fig. 14 for the infinite grating.

respectively, computed with only the real parts of the impedances, given in Table I. Our setting the imaginary parts of the impedances to zero results in a significant drop in grating performance. The reflection and transmission coefficients that were zeroed out with the complex impedance now assume high values, exceeding the

transmission coefficient of the  $n = -1$  diffracted mode in all cases. This contrasts with the linear clusters, for which the effect of setting  $\text{Im}\mu_\alpha = 0$  is minimal; see Figs. 7 and 8. The difference can be explained by the observation from Table I that the impedances of the linear clusters are all lightly damped, while each of the

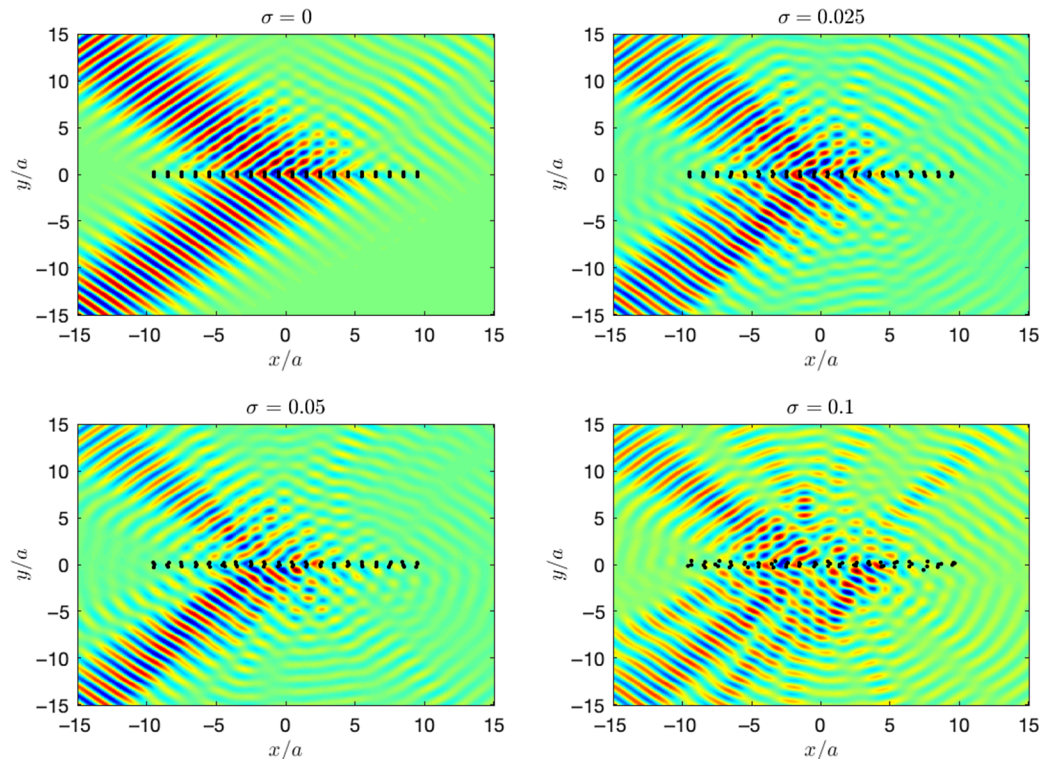


FIG. 16. Multiple-scattering simulations of finite gratings under Gaussian-beam excitation. The parameter  $\sigma$  represents the degree of random disorder that has been added to all the scatterers of the cluster.

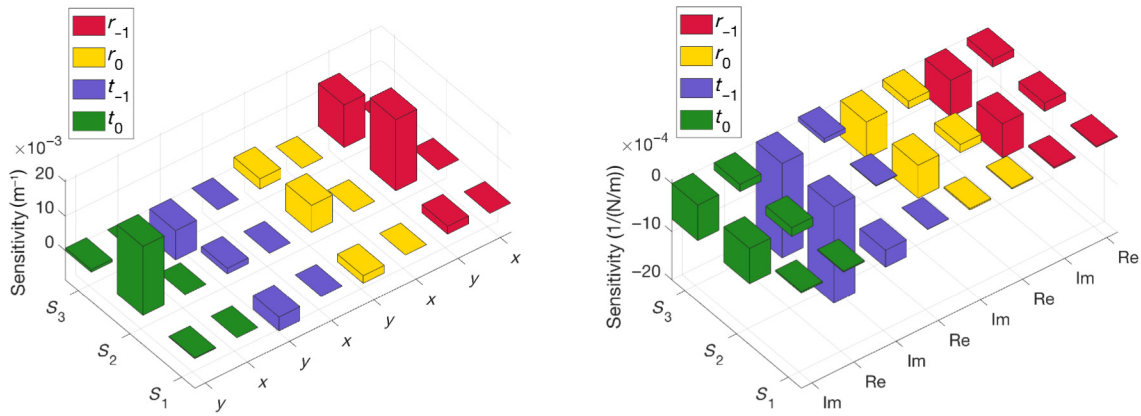


FIG. 17. Sensitivity parameters for linear cluster 1 ( $d = 0.225, \theta_d = \pi/2$ ): (a) sensitivity parameters for individual changes in scatterers' ( $S_1$ – $S_3$ ) positions ( $x$  and  $y$ ) for the four reflection and transmission coefficients of the diffracted modes (for fixed  $\mu$ ); (b) sensitivity parameters for individual changes in scatterers' real and imaginary parts of impedances ( $\mu_1$ – $\mu_3$ ) for the four diffracted modes reflection and transmission coefficients (fixed  $S_1$ – $S_3$  positions).

triangular clusters has one impedance that is significantly damped.

### 3. Infinite and finite retroreflector gratings with disorder

Figure 14 shows the field distributions for the designed  $N = 3$  gratings. The upper panels show the simulation of an incident plane wave from the negative  $y$  direction with angle of incidence  $\theta_0 = \pi/4$  and incident wavenumber for the different configurations defined in Table I. The lower panels show results for the same cluster after our setting the imaginary part equal to zero. The negative refraction is evident in the simulations, and it is clear as well that the larger the imaginary part of  $\mu_\alpha$ , the weaker the refracted wave. This is a consequence of the loss of wave energy caused by the highly damped resonators, although it is noted that

the channeling of all the energy toward the  $n = -1$  mode is still efficient in the sense that other modes are zeroed out, as designed. Overall, we see how ignoring the imaginary part has no visible effect in the linear cluster but drastically diminishes the amplitude of the refracted mode in the triangular clusters. As noted above, the reason for this may be understood from the fact that scatterers of the linear clusters are lightly damped but the triangular clusters have at least one highly damped impedance; see Table I.

Finally, Figs. 15 and 16 demonstrate that the effects predicted for the infinite grating are robust under finite limitations on the grating size, for finite incident beams, and in the presence of positional disorder. Thus, the same effects as observed for the infinite grating in Fig. 14 are apparent in Fig. 15, which shows the total field for incidence

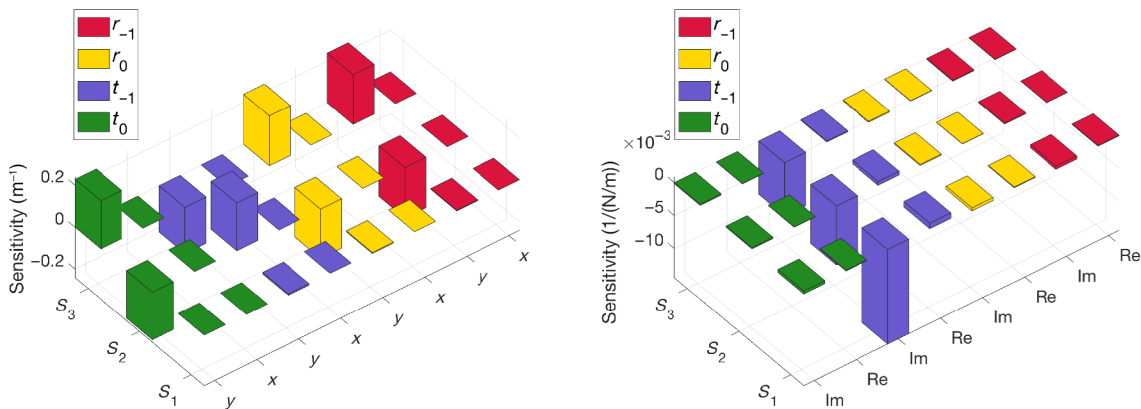


FIG. 18. Sensitivity parameters for linear cluster 2 ( $d = 0.75, \theta_d = \pi/2$ ): (a) sensitivity parameters for individual changes in scatterers' ( $S_1$ – $S_3$ ) positions ( $x$  and  $y$ ) for the four reflection and transmission coefficients of the diffracted modes (for fixed  $\mu$ ); (b) sensitivity parameters for individual changes in scatterers' real and imaginary parts of impedances ( $\mu_1$ – $\mu_3$ ) for the four diffracted modes reflection and transmission coefficients (fixed  $S_1$ – $S_3$  positions).

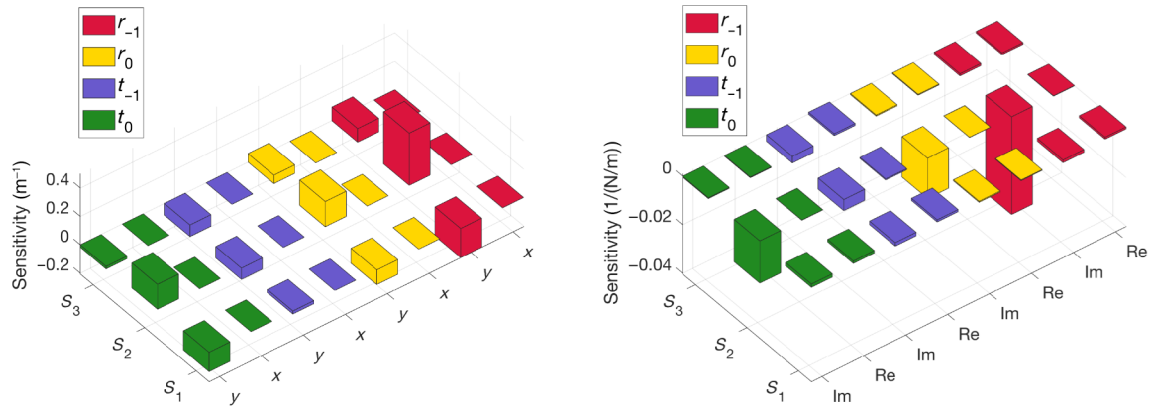


FIG. 19. Sensitivity parameters for triangular cluster 1 ( $d = 0.75$ ,  $\theta_d = 0.92$ ): (a) sensitivity parameters for individual changes in scatterers' ( $S_1$ – $S_3$ ) positions ( $x$  and  $y$ ) for the four reflection and transmission coefficients of the diffracted modes (for fixed  $\mu$ ); (b) sensitivity parameters for individual changes in scatterers' real and imaginary parts of impedances ( $\mu_1$ – $\mu_3$ ) for the four diffracted modes reflection and transmission coefficients (fixed  $S_1$ – $S_3$  positions).

on a finite grating of 30 clusters of the linear and triangular configurations. The same finite configuration is considered in Fig. 16 for Gaussian-beam incidence and for imperfections in the grating. The simulations indicate that good agreement with the infinite system under plane-wave incidence is expected for zero and small levels of disorder.

## V. PRACTICAL CONSIDERATIONS ON SCATTERERS AND CLUSTERS

The grating performance, in terms of its reflection and transmission properties, depends on deviations of actual operation conditions from designed ones. Here we consider the performance as a function of deviations in scatterer positions, impedances, and the operating wavelength.

Anomalous refractors and reflectors are obviously narrowband, since the effect is due to diffraction, which by definition is wavelength dependent [see Eq. (24)]. However, this dependence is smooth, so small deviations from the angle of incidence or desired wavelength produce small deviations in the diffracted angle. This is also true for the channeling of energy; as can be seen in Figs. 7 and 8, the frequency dependence of the energy exchange between modes is smooth around the optimal value. Small variations about the optimal point produce small additional scattered waves, while the overall effect remains unchanged.

We have already seen in in Figs. 7, 8, 12, and 13 how the reflection and transmission coefficients depend on changes in the incident wavenumber for linear and triangular

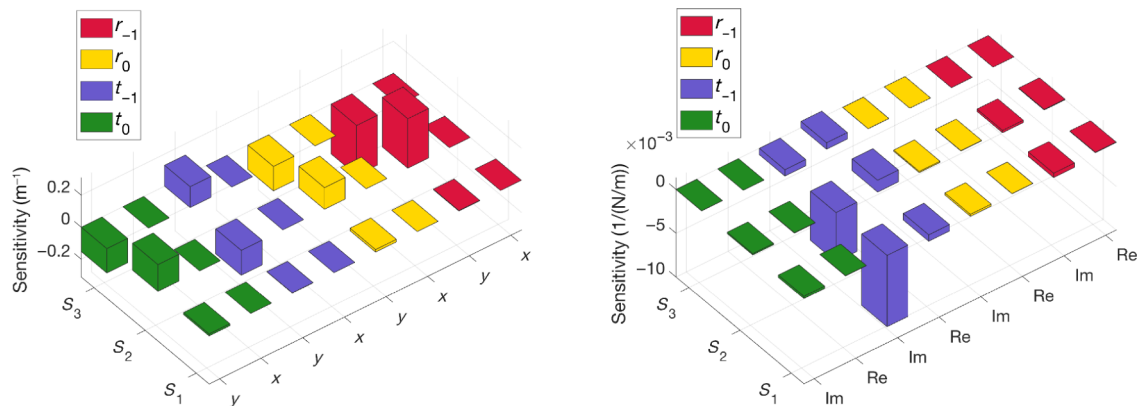


FIG. 20. Sensitivity parameters for triangular cluster 2 ( $d = 0.75$ ,  $\theta_d = 0.92$ ): (a) sensitivity parameters for individual changes in scatterers' ( $S_1$ – $S_3$ ) positions ( $x$  and  $y$ ) for the four reflection and transmission coefficients of the diffracted modes (for fixed  $\mu$ ); (b) sensitivity parameters for individual changes in scatterers' real and imaginary parts of impedances ( $\mu_1$ – $\mu_3$ ) for the four diffracted modes reflection and transmission coefficients (fixed  $S_1$ – $S_3$  positions).

clusters, respectively. Figures 17–18 illustrate the influence of changes in scatterer positions [Figs. 17(a), 18(a), 19(a), and 20(a)] and impedances [real and imaginary parts, Figs. 17(b), 18(b), 19(b), and 20(b)] on reflection and transmission coefficients for the linear and triangular clusters.

These sensitivity studies show that dependence on the horizontal ( $x$ ) positions of the grating scatterers is negligible. They also indicate that linear clusters display small sensitivity to the position of the central scatterer. Linear cluster 1 (i.e., a linear configuration with small scatterer spacing) shows sensitivity measures related to position changes that are 2 orders of magnitude smaller than for the other clusters (linear cluster 2 and triangular clusters 1 and 2). The target transmitted mode coefficient,  $t_{-1}$ , is the least-sensitive parameter to changes in the scatterers' positions [see Figs. 17(a), 18(a), 19(a), and 20(a)], meaning that grating performance will be affected more by increase in other diffracted-mode amplitudes than by decrease in the target-mode amplitude,  $t_{-1}$ .

In general, it can be seen that for both cluster types (i.e., linear and triangular) small (negligible) variations in reflection and transmission coefficients are expected for small shifts of all scatterers' positions, as shown in Figs. 17(a), 18(a), 19(a), and 20(a). Also, for the impedance values given in Table I, the relatively small impact of changes in impedances (real and imaginary parts) on reflection and transmission coefficients can be seen from Figs. 17(b), 18(b), 19(b), and 20(b). For both cluster types, damping properties are critical to the grating performance. For the two linear clusters considered and triangular cluster 2, it is seen that damping—related to the imaginary part of impedance—has the highest influence on  $t_{-1}$ .

## VI. SUMMARY

We describe a general approach for the inverse design of gratings for flexural waves in thin plates. Using a one-dimensional periodic arrangement of clusters of a finite number of point attachments, one can channel the incident energy toward a desired direction. The general solution for the inverse problem requires a cluster of both active and passive attachments; however, it is possible to find solutions with only passive point scatterers. The required mechanical properties of the attached scatterers are defined by the impedances, which are obtained by our solving a linear system of equations. We show through specific examples that some configurations, the linear clusters, possess very low dissipation, resulting in very high conversion to the desired refracted mode. It should be noted that the impedances of the cluster elements are linearly related to the desired diffraction parameters; the design process requires only a matrix inversion. The present approach, although derived for flexural waves and for the specific

example of the negative refractor, can be easily exported to other waves and devices.

## ACKNOWLEDGMENTS

A.N.N. acknowledges support from the National Science Foundation under Grant No. EFRI 1641078 and the Office of Naval Research under MURI Grant No. N00014-13-1-0631. P.P. acknowledges support from the National Centre for Research and Development under the LIDER research programme (Project No. LIDER/317/L-6/14/NCBR/2015). D.T. acknowledges financial support through a “Ramón y Cajal” fellowship under grant number RYC-2016-21188 and by the U.S. Office of Naval Research under Grant No. N00014-17-1-2445.

## APPENDIX A: PLATE GREEN'S FUNCTION

The Green's function, which satisfies

$$D[\Delta^2 G(\mathbf{r}) - k^4 G(\mathbf{r})] = \delta(\mathbf{r}), \quad (\text{A1})$$

can be readily obtained with use of a double Fourier transform as

$$G(\mathbf{r}) = \frac{1}{D(2\pi)^2} \int_{\mathbb{R}^2} \frac{e^{i(\xi x + \eta y)} d\xi d\eta}{(\xi^2 + \eta^2)^2 - k^4}. \quad (\text{A2})$$

Evaluation of the  $\eta$  integral with use of the Cauchy residue theorem gives

$$G(\mathbf{r}) = \frac{1}{2\pi} \int_{\mathbb{R}} d\xi e^{i\xi x} f(\xi, y), \quad (\text{A3a})$$

$$f(\xi, y) = \frac{1}{4Dk^2} \left[ \frac{e^{-(\xi^2 - k^2)^{1/2}|y|}}{(\xi^2 - k^2)^{1/2}} - \frac{e^{-(\xi^2 + k^2)^{1/2}|y|}}{(\xi^2 + k^2)^{1/2}} \right]. \quad (\text{A3b})$$

Note that  $(\xi^2 - k^2)^{1/2} = -i\sqrt{k^2 - \xi^2}$  for  $|\xi| < k$ . The explicit form [Eq. (6)] follows with use of known integral representations for the Hankel function.

The line sum

$$\sum_{m \in \mathbb{Z}} e^{ik_x m a} G(\mathbf{r} - m a \hat{\mathbf{x}}) = \sum_{m \in \mathbb{Z}} \frac{1}{2\pi} \int_{\mathbb{R}} d\xi e^{i m a (k_x - \xi)} e^{i\xi x} f(\xi, y) \quad (\text{A4})$$

can be simplified with use of the Poisson summation formula

$$\sum_{m \in \mathbb{Z}} \frac{1}{2\pi} \int_{\mathbb{R}} du e^{\pm i m u} F(u) = \sum_{n \in \mathbb{Z}} F(2\pi n). \quad (\text{A5})$$

Hence,

$$\sum_{m \in \mathbb{Z}} e^{ik_x m a} G(\mathbf{r} - m a \hat{\mathbf{x}}) = \frac{1}{a} \sum_{n \in \mathbb{Z}} e^{i[k_x + (2\pi/a)n]x} \times f\left(k_x + \frac{2\pi}{a}n, y\right), \quad (\text{A6})$$

with  $f$  defined in Eq. (A3b). This gives the identity (19).

### APPENDIX B: THE $N = 3$ RETROREFLECTOR GRATING, LINEAR CLUSTER

If we assume a configuration of  $N = 3$  scatterers and use the fact that  $\mathbf{k}_{-1}^{\pm} = -\mathbf{k}_0^{\mp}$  for the negative refractor, Eq. (47) becomes

$$\hat{\mathbf{S}} = \frac{iG_0}{k \sin \theta_0} \begin{pmatrix} 1 & e^{-ik_0^+ \cdot \mathbf{R}_2} & e^{-ik_0^+ \cdot \mathbf{R}_3} \\ 1 & e^{-ik_0^- \cdot \mathbf{R}_2} & e^{-ik_0^- \cdot \mathbf{R}_3} \\ 1 & e^{ik_0^+ \cdot \mathbf{R}_2} & e^{ik_0^+ \cdot \mathbf{R}_3} \end{pmatrix}. \quad (\text{B1})$$

Taking  $\mathbf{R}_2 = \mathbf{R}_+$  and  $\mathbf{R}_3 = \mathbf{R}_-$ , where  $\mathbf{R}_{\pm} = \pm d(\cos \theta_d, \sin \theta_d)$ , we have

$$\hat{\mathbf{S}} = \frac{iG_0}{k \sin \theta_0} \begin{pmatrix} 1 & e^{-i\phi_-} & e^{i\phi_-} \\ 1 & e^{-i\phi_+} & e^{i\phi_+} \\ 1 & e^{i\phi_-} & e^{-i\phi_-} \end{pmatrix}, \quad (\text{B2})$$

where  $\phi_{\pm} = kd \cos(\theta_d \pm \theta_0)$ . Note that

$$\begin{aligned} \det \hat{\mathbf{S}} &= \frac{4G_0^3}{(k \sin \theta_0)^3} (\cos \phi_- - \cos \phi_+) \sin \phi_- \\ &= -\left(\frac{2G_0}{k \sin \theta_0}\right)^3 \sin[kd \cos(\theta_d - \theta_0)] \\ &\quad \times \sin(kd \cos \theta_d \cos \theta_0) \sin(kd \sin \theta_d \sin \theta_0), \end{aligned} \quad (\text{B3})$$

which clearly vanishes at the ‘‘forbidden’’ values  $\theta_d = 0$ ,  $\pi/2$ , and  $\pi$ . However, with reference to Eq. (41),

$$\hat{\mathbf{S}}^{-1} \mathbf{e}_1 = \frac{k \sin \theta_0}{4iG_0 \sin \phi_- \sin \frac{1}{2}(\phi_+ - \phi_-)} \times \begin{pmatrix} -2 \cos \frac{1}{2}(\phi_+ + \phi_-) \\ e^{i(\phi_+ - \phi_-)/2} \\ e^{i(\phi_- - \phi_+)/2} \end{pmatrix}, \quad (\text{B4})$$

which is well defined for  $\theta_d = \pi/2$  even though  $\det \hat{\mathbf{S}} = 0$  at that angle.

[1] Younes Ra’di, Dimitrios L. Sounas, and Andrea Alu, Metagratings: Beyond the Limits of Graded Meta Surfaces for Wave Front Control, *Phys. Rev. Lett.* **119**, 067404 (2017).

- [2] Ariel Epstein and Oshri Rabinovich, Unveiling the Properties of Metagratings via a Detailed Analytical Model for Synthesis and Analysis, *Phys. Rev. Appl.* **8**, 054037 (2017).
- [3] Alex M. H. Wong and George V. Eleftheriades, Perfect Anomalous Reflection with a Bipartite Huygens’ Metasurface, *Phys. Rev. X* **8**, 011036 (2018).
- [4] Li Quan, Younes Ra’di, Dimitrios L. Sounas, and Andrea Alu, Maximum Willis Coupling in Acoustic Scatterers, *Phys. Rev. Lett.* **120**, 254301 (2018).
- [5] Oshri Rabinovich and Ariel Epstein, Analytical design of printed-circuit-board (PCB) meta-gratings for perfect anomalous reflection, arXiv:1801.04521 (2018).
- [6] Ariel Epstein and Oshri Rabinovich, Perfect anomalous refraction with metagratings, arXiv:1804.02362 (2018).
- [7] Nanfang Yu, Patrice Genevet, Mikhail A. Kats, Francesco Aieta, Jean-Philippe Tetienne, Federico Capasso, and Zeno Gaburro, Light propagation with phase discontinuities: Generalized laws of reflection and refraction, *Science* **334**, 333 (2011).
- [8] Daniel Torrent, Acoustic anomalous reflectors based on diffraction grating engineering, *Phys. Rev. B* **98**, 060101 (2018).
- [9] D. V. Evans and R. Porter, Penetration of flexural waves through a periodically constrained thin elastic plate in vacuo and floating on water, *J. Eng. Math.* **58**, 317 (2007).
- [10] Yong Xiao, Jihong Wen, and Xisen Wen, Flexural wave band gaps in locally resonant thin plates with periodically attached spring-mass resonators, *J. Phys. D: Appl. Phys.* **45**, 195401 (2012).
- [11] Daniel Torrent, Didier Mayou, and José Sánchez-Dehesa, Elastic analog of graphene: Dirac cones and edge states for flexural waves in thin plates, *Phys. Rev. B* **87**, 115143 (2013).
- [12] Raj Kumar Pal and Massimo Ruzzene, Edge waves in plates with resonators: An elastic analogue of the quantum valley hall effect, *New J. Phys.* **19**, 025001 (2017).
- [13] N. V. Movchan, R. C. McPhedran, A. B. Movchan, and C. G. Poulton, Wave scattering by platonic grating stacks, *Proc. R. Soc. A: Math. Phys. Eng. Sci.* **465**, 3383 (2009).
- [14] S. G. Haslinger, N. V. Movchan, A. B. Movchan, and R. C. McPhedran, Transmission, trapping and filtering of waves in periodically constrained elastic plates, *Proc. R. Soc. A: Math. Phys. Eng. Sci.* **468**, 76 (2011).
- [15] S. G. Haslinger, N. V. Movchan, A. B. Movchan, I. S. Jones, and R. V. Craster, Controlling flexural waves in semi-infinite platonic crystals with resonator-type scatterers, *Q. J. Mech. Appl. Math.* **70**, 216 (2017).
- [16] Vitaliy E. Gusev and Oliver B. Wright, Double-negative flexural acoustic metamaterial, *New J. Phys.* **16**, 123053 (2014).
- [17] Daniel Torrent, Yan Pennec, and Bahram Djafari-Rouhani, Effective medium theory for elastic metamaterials in thin elastic plates, *Phys. Rev. B* **90**, 104110 (2014).
- [18] M. Farhat, S. Guenneau, and S. Enoch, High directivity and confinement of flexural waves through ultra-refraction in thin perforated plates, *EPL* **91**, 54003 (2010).
- [19] Michael J. A. Smith, Ross C. McPhedran, Chris G. Poulton, and Michael H. Meylan, Negative refraction and dispersion



- phenomena in platonic clusters, *Waves Random Complex Media* **22**, 435 (2012).
- [20] M. H. Meylan and R. C. McPhedran, Fast and slow interaction of elastic waves with platonic clusters, *Proc. R. Soc. A: Math. Phys. Eng. Sci.* **467**, 3509 (2011).
- [21] A. B. Movchan, N. V. Movchan, and R. C. McPhedran, Bloch-Floquet bending waves in perforated thin plates, *Proc. R. Soc. A: Math. Phys. Eng. Sci.* **463**, 2505 (2007).
- [22] M. J. Brennan, Vibration control using a tunable vibration neutralizer, *Proc. Inst. Mech. Eng. Part C: J. Mech. Eng. Sci.* **211**, 91 (1997).
- [23] M. J. Brennan, Control of flexural waves on a beam using a tunable vibration neutraliser, *J. Sound Vib.* **222**, 389 (1999).
- [24] H. M. El-Khatib, B. R. Mace, and M. J. Brennan, Suppression of bending waves in a beam using a tuned vibration absorber, *J. Sound Vib.* **288**, 1157 (2005).